Interface charge transfer in polypyrrole coated perovskite manganite magnetic nanoparticles

O. Pana, M. L. Soran, C. Leostean, S. Macavei, E. Gautron et al.

Citation: J. Appl. Phys. **111**, 044309 (2012); doi: 10.1063/1.3686662
View online: http://dx.doi.org/10.1063/1.3686662
View Table of Contents: http://jap.aip.org/resource/1/JAPIAU/v111/i4
Published by the American Institute of Physics.

Interface charge transfer in polypyrrole coated perovskite manganite magnetic nanoparticles

O. Pana,[1] M. L. Soran,[1,a)] C. Leostean,[1] S. Macavei,[1] E. Gautron,[2] C. M. Teodorescu,[3] N. Gheorghe,[3] and O. Chauvet[2]
[1]*National Institute for R&D of Isotopic and Molecular Technologies, PO Box 700, 400293 Cluj-Napoca, Romania*
[2]*Institute of Materials Jean Rouxel Nantes, 44322 Nantes cedex 3, France*
[3]*National Institute for R&D of Material Physics, 105 Atomistilor st., 077125 Bucharest -Magurele, Romania*

(Received 3 October 2011; accepted 19 January 2012; published online 22 February 2012)

Different hybrid structures were obtained by coating magnetic nanoparticles of perovskite type manganite at optimal doping ($La_{0.67}Sr_{0.33}MnO_3$,LSMO) with different quantities of polypyrrole (PPy). The amorphous layer of polypyrrole surrounding the crystalline magnetic core was observed by high resolution transmission electron microscopy (HRTEM) and analyzed by using X-ray photoelectron spectroscopy (XPS) and X-ray absorption spectroscopy (XAS) measurements in near edge structure (XANES) techniques. By analyzing the magnetic behavior of the samples one can observe that the surface modification of magnetic nanoparticles by PPy results in an increase in the saturation magnetization of the composites. The process is ascribed to paired electrons transferred from the delocalized π states of the PPy into the outer disordered layers of the manganite. The analysis of pre-edge peak of the Mn K-edge XANES spectra in the case of PPy coated LSMO nanoparticles indicates that the charge transfer between polymer and nanoparticles is (directed) going to missing or distorted oxygen positions, hence increasing the 3*d* electrons' mobility and orbital hybridization between the neighboring manganese ion. As a consequence, within the surface layers of LSMO nanoparticles, both energy bands disrupted the structure, and the double exchange process between Mn ions was reestablished determining the saturation magnetizations and pre-edge features increase, respectively. © *2012 American Institute of Physics*. [doi:10.1063/1.3686662]

I. INTRODUCTION

The development of magnetic core-shell nanoparticles with a magnetic core and a polymeric shell offers the advantage of tailoring the magnetic properties and functionalizing the magnetic particles. The combination of conducting polymers and inorganic magnetic nanoparticles produces various nanocomposites with the specific properties required by a wide range of applications in the following: biotechnology, electromagnetic interference shielding, microwave absorbing, magnetic separation.[1–3]

Surface modification of magnetic nanoparticles by coating with surfactants or polymers may produce important changes of their magnetic properties.[4,5] By adjusting the coating layers, one can induce changes in the nanoparticles' surface spin disorder and interparticle interactions; this results in different values for the characteristic parameters like saturation magnetization, coercitivity, and magnetic anisotropy of the nanoparticles obtained by different procedures.[6–12]

In this work, we report the synthesis and characterization of novel core-shell hybrid organic-inorganic nanostructures, consisting in the deposition of a conjugated polymer layer on the magnetic $La_{0.67}Sr_{0.33}MnO_3$ (LSMO) nanoparticle surfaces. We focus especially on the polymer nanoparticle interface-properties' relationship and optimization of the nanocomposites physicochemical characteristics to make them suitable for biotechnology. Different hybrid structures were obtained by coating magnetic LSMO nanoparticles with different shell thickness of polypyrrole (PPy). The thin amorphous layer of polypyrrole surrounding the crystalline magnetic core was observed by high resolution transmission electron microscopy (HRTEM) and analyzed by using X-ray photoelectron spectroscopy (XPS), magnetic measurements, and XAS techniques. The surface modification of magnetic nanoparticles by PPy coatings results in an increase in the saturation magnetization that can be correlated with the XANES pre-edge absorption peaks of the Mn-K edge.

II. EXPERIMENTAL

A. Samples preparation

A two step procedure was used to obtain these novel core-shell nanostructures. First, the $La_{0.67}Sr_{0.33}MnO_3$ (LSMO) manganite was prepared by a sol-gel procedure using diethylenetriaminepentaacetic acid as the gelling agent.[13–16] The corresponding metallic oxides and $Mn(CH_3COO)_2$ H_2O, in the necessary stoichiometric ratio, were used as precursors. They were introduced in HNO_3 aqueous solution to obtain the corresponding nitrates. The molar ratio metal: gelling agent was set to 1:1.5. The reaction mixture was evaporated for 24 h at 250 °C, and a black powder was obtained. This powder was

a)Author to whom correspondence should be addressed. Electronic mail: loredana.soran@itim-cj.ro.

annealed for 2 h at 700 °C, and then it was used for the preparation of core-shell LSMO@PPy nanocomposites.

The magnetic nanocomposites based on polypyrrole were prepared by oxidative polymerization of pyrrole (Py) in aqueous solution using ammonium peroxodisulfate (APS) as an oxidant in the water based manganite. As seen in Table I, an oxidant/pyrrole molar ratio Ox/Py = 0.2 and various ratios of Py/LSMO were used for the preparation of the investigated samples. LSMO nanoparticles were sonicated for 1 h at 80 °C in water with or without oleic acid (11.7 mmol). After decreasing the temperature below 10 °C, the other reagents were added in the solution. The polymerization reaction time was 5 h. The resulted samples appeared as a black precipitate. Each sample was washed with methanol, water, and again with methanol. Finally, there were dried in an oven at 60 °C. Changing Py/LSMO ratios between 0.66 and 10, three samples, labeled 1–3, were prepared by using this method. The initial ratios utilized in the synthesis are shown in the second and third columns of Table I. LSMO nanoparticles uncovered with PPy were also kept for comparison (sample labeled LSMO).

B. Characterization methods

The morphology of the magnetic nanoparticles and of the PPy based magnetic nanocomposites was determined by transmission electron microscopy (TEM) and high resolution TEM (HRTEM) using 1010 JEOL and Hitachi H9000NAR transmission electron microscopes. X-ray photoelectron spectroscopy (XPS) associated with Ar ion etching was used for qualitative and quantitative compositional analysis of nanocomposites, using a SPECS custom built system. The magnetic characterization of bare LSMO and PPy coated magnetic nanoparticles was recorded by using a vibrating sample magnetometer (VSM) produced by Cryogenic Ltd. The temperature dependence of the magnetization at a low applied field (0.01 T) under zero-field cooling (ZFC) and field-cooling (FC) conditions was determined using a Quantum Design commercial SQUID magnetometer (MPMS XL7). X-ray absorption spectroscopy (XAS) measurements in near edge structure (XANES) region were performed at the Hasylab synchrotron radiation facility at DESY, Hamburg, on beamline A1 of the Doris III storage ring. Powder samples were pressed into pellets with cellulose and measured in transmission mode.

TABLE I. Initial synthesis conditions for LSMO@PPy samples and weight contents as resulted from XPS analysis.

	Synthesis conditions		Weight contents resulted from XPS		
Sample	Py/LSMO molar ratio	Oleic acid as surfactant	LSMO wt%	PPy wt%	Oleic acid wt%
LSMO	–	yes	96.3	–	3.7
LSMO@PPy 1	0.66	yes	82.8	14.3	2.9
LSMO@PPy 2	3.33	no	43.7	56.3	–
LSMO@PPy 3	10	yes	22.2	68.3	9.5

III. RESULTS AND DISCUSSIONS

As an example, HRTEM images of the magnetic nanocomposites are given in Fig. 1(a). Figure 1(b) represents an enhanced detail of one nanoparticle from Fig. 1(a). One can observe that the darker LSMO nanoparticles are surrounded by a clearer layer of polymer. This layer is approximately 1.5–3.5 nm thick. Different crystalline atomic planes can be distinguished for some nanoparticles. The distance between the atomic planes, as seen in Fig. 1(b), is about 2.15 Å and corresponds to the (100) family planes. Also, in Fig. 1(b), one can observe that the polymer surrounding the LSMO nanoparticle seems to be strongly adhesive onto its surface, thus resulting into a very intimate core-shell connection between the two components. As a consequence, an important interaction between PPy and the surface layers of the

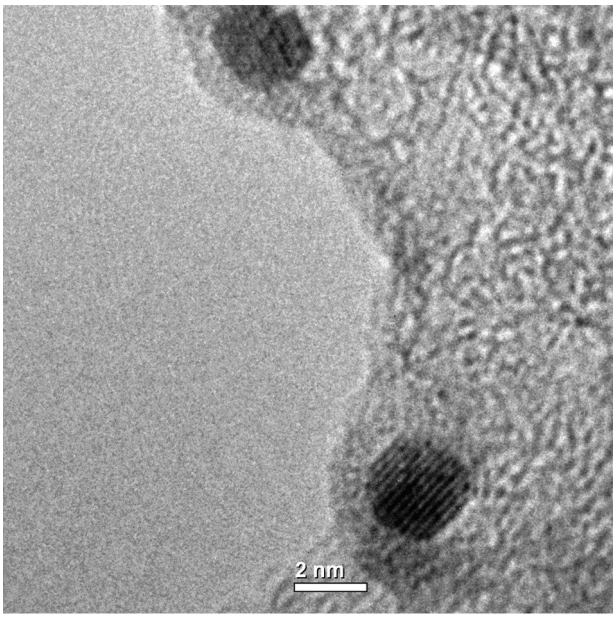

(*a*)

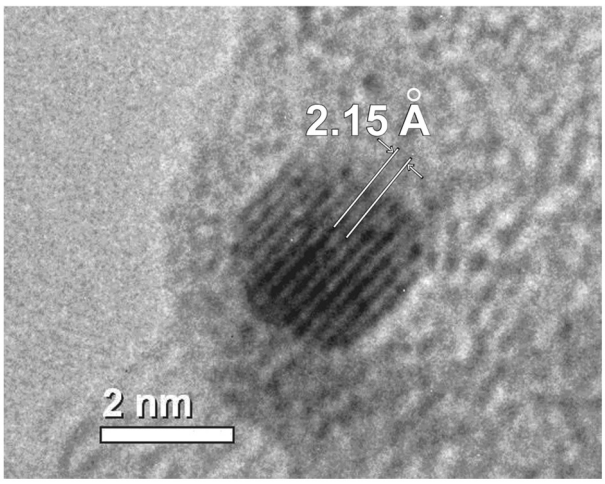

(*b*)

FIG. 1. (a) HRTEM images of LSMO nanoparticles covered with PPy. (b) Enhanced detail evidencing the core-shell structure resulted by PPy attachment. The atomic planes corresponding to the (100) family of LSMO can be seen in (b).

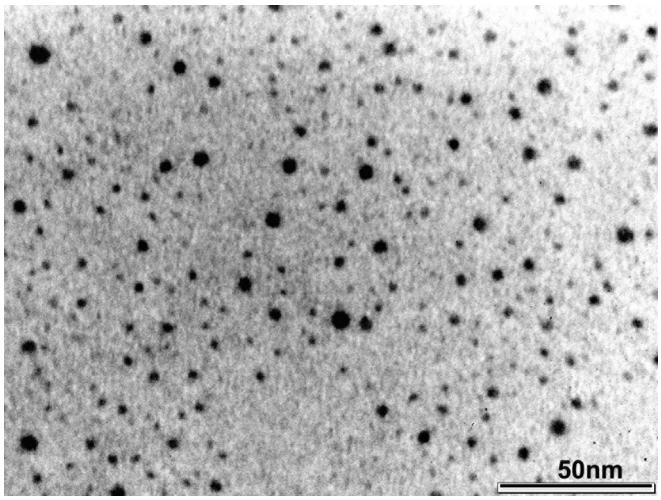

FIG. 2. TEM image of an ensemble of LSMO nanoparticles covered with PPy. Spherical bundles wrapped within a polymeric "cloud" can be observed in certain cases.

nanoparticles is expected to occur. A TEM ensemble image is presented in Fig. 2 where one can observe that, in certain cases, the nanoparticles show some of the tendency to form spherical bundles wrapped within a polymeric "cloud." This could be attributed to dipolar magnetic interactions favoring the cluster formation.

The compositions of PPy coated LSMO nanoparticle samples were determined by using the XPS technique. The excitation was made by using the Al anode of the X-rays source ($h\upsilon = 1486.6$ eV). The manganese $2p$ and the pyrrolic nitrogen $1s$ core-levels peaks were used for quantitative determinations. The nitrogen content was also correlated with the carbon concentrations belonging to the polymeric chains (C $1s$ core-level). Additional carbon is present in spectra due to the oleic acid as surfactant molecules. As an example, the recorded XPS spectra of Mn $2p$ core-level doublet of sample 3 together with the corresponding deconvolutions and the fitted curve are shown in Fig. 3. In the manganese case, the deconvolution was realized by using Mn^{3+} and Mn^{4+} doublet states as components. In Fig. 3, the Mn^{3+} and Mn^{4+} peaks are labeled A and B, respectively.

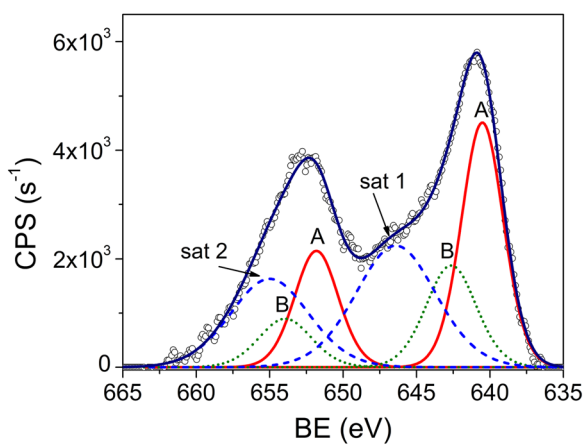

FIG. 3. (Color online) XPS recorded spectrum of Mn *2 p* core-level doublet of the LSMO@PPy 1 sample together with corresponding deconvolutions and fitted curves. Peaks labeled A and B correspond to $Mn^{3+}$and Mn^{4+}, respectively. Two shake-up satellites are also present in the spectrum.

As expected, two additional satellite peaks, situated at around 653 eV and 656 eV, respectively, were also seen.[17] The restrictions used for the fit of Mn $2p$ XPS spectra refer to the relation between areas of the two components, $A_{1/2} = A_{3/2}/2$. The ratios between (3/2) and (1/2) line widths were set between 1 and 1.1. The integral intensities were calibrated by using the real sensitivity, transmission, and electronic mean free path factors. The calculation of the corresponding weight concentrations were made by dividing the integral intensities to the specific attenuation lengths of each component of the hybrid system.

The values of the attenuation lengths were calculated upon Cumpson and Seah[18] and are as follows: 0.985 nm for LSMO concerning Mn $2p$ core-level, 2.3 nm and 2.14 nm for PPy and oleic acid, respectively, as referring to the C $1s$ core-level peaks. The weight contents of LSMO, PPy, and oleic acid in case of the composite samples, as determined by XPS, are shown in Table I. The knowledge of the weight content of manganite in each sample is necessary for the absolute calculation of magnetizations.

The magnetization curves at room temperature of the bare LSMO nanoparticles together with the LSMO/PPy nanocomposites are presented in Fig. 4. The values of the magnetizations are normalized to the LSMO content of each specific nanocomposite according to Table I. As expected, the magnetization of different combinations of PPy and LSMO nanoparticles together with the bare LSMO nanoparticles covered or not with oleic acid as surfactant shows only a very small hysteresis loop, which is consistent with superparamagnetic behavior.[19] The continuous lines represent the best fit based on the following equation:[20]

$$M(H,T) = M_S \frac{\int V(D_m) L\left[\frac{M_S V(D_m) H}{k_B T}\right] f(D_m) dD_m}{\int V(D_m) f(D_m) dD_m}. \quad (1)$$

Here $V(D_m)$ is the volume of the magnetic core of the nanoparticles expressed as a function of diameters D_m ("magnetic"

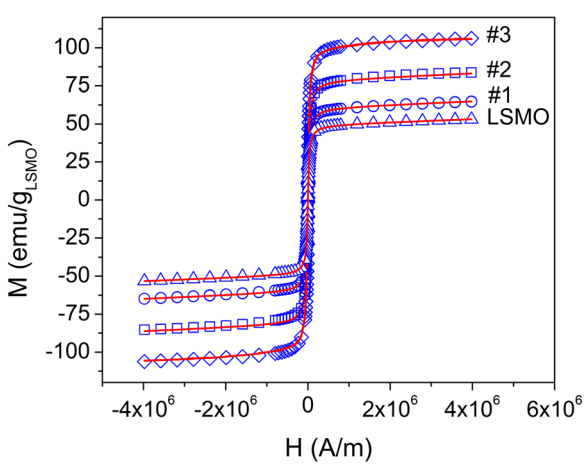

FIG. 4. (Color online) The magnetization curves vs applied magnetic field at room temperature of the LSMO@PPy samples 1-3 and bare LSMO nanoparticle samples. The absolute magnetizations are calculated referred to the LSMO content of each specific sample. The continuous lines represent the best fits obtained for each sample using Eq. (1).

TABLE II. The calculated values of weight contents of the samples as resulted from XPS data. The last column contains the number of Bohr magnetons per formula unit, μ_s calculated from M_S.

Sample	D_m (nm)	σ_m	M_S (emu/g of $La_{0.67}Sr_{0.33}MnO_3$)	μ_S (μ_B/f.u.)
LSMO	9.90*	0.175[a]	49.4[a]	2.0
LSMO@PPy 1	8.90	0.150	60.8	2.44
LSMO@PPy 2	8.05	0.185	80.5	3.24
LSMO@PPy 3	7.20	0.230	102.0	4.12

[a]Values for bare LSMO nanoparticles were taken from Pana *et al.* (Ref. 21).

diameter), H is the applied external magnetic field, and $f(D_m)$ is the distribution of diameters (usually a lognormal distribution is considered). The calculations were performed following the method presented in Turcu *et al.*[12] The data fit was realized selecting, for instance, only points corresponding to the increasing magnetic field from the M(H) dependence. By utilizing decreasing magnetic field data, the results of the fitting process were the same. This is due to the fact that at room temperature, the coercive field has indeed very small values. Even if the system has a superparamagnetic behavior both coercive field and remanent magnetization are present in the M(H) dependences. They have very small values as compared to usual ferromagnetic behavior. For our samples, at room temperature, H_C has values of about ~15 Oe, being three orders of magnitude smaller than the field value at which the saturation process begins. H_C values increase with decreasing temperature. For all the composite and LSMO samples, the corresponding remanent magnetizations are also very small: 1.7 – 0.5 emu/g and 12.0 – 5.9 emu/g at room temperature and 4.2 K, respectively. Therefore the area inside the hysteresis loop is small but not zero. For instance, the hyperthermic effect is mainly based on this peculiar feature.

The fit parameters were: the magnetic mean size distribution parameter D_{0m}, the dispersion σ_m and the saturation magnetization M_S. The calculated values are presented in Table II. The saturation magnetizations were normalized to the corresponding LSMO content (column 4) and the number of Bohr magnetons per formula unit, μ_s, was calculated by using the values of M_S.

Several facts should be noticed concerning the data shown in Table II. First, by comparing the calculated magnetic diameters D_{0m} with the diameters D_0 as they resulted from the analysis of TEM images of bare LSMO nanoparticles and presented in Pana *et al.*,[21] one can observe that the calculated diameters are twice larger that the real values D_0. This fact represents an indication that due to the dipole-dipole magnetic interactions between nanoparticles, there is a tendency for cluster formation, each particle apparently having a much larger magnetic diameter that the real one.[21]

To further check this hypothesis, the temperature dependences of the magnetizations in the field-cooled (FC) and zero-field cooled (ZFC) regimes for the LSMO nanoparticles and the LSMO@PPy core-shell systems were measured and analyzed. The ZFC-FC data are presented in Fig. 5.

In the superparamagnetic regime, the difference between FC and ZFC gives the thermo-remanent magnetizations (TRMs). This way, starting from low temperatures and warming up the system, the deblocking process of magnetizations begins first with small particles after which larger particles are involved. This way, for any reached temperature, the value of TRM represents the sum of the nanoparticle magnetic moments that are still blocked. Deblocking occurs when the thermal energy overcomes the anisotropy energy barrier ΔE_a.[25] In certain cases, an additional magnetic interaction like

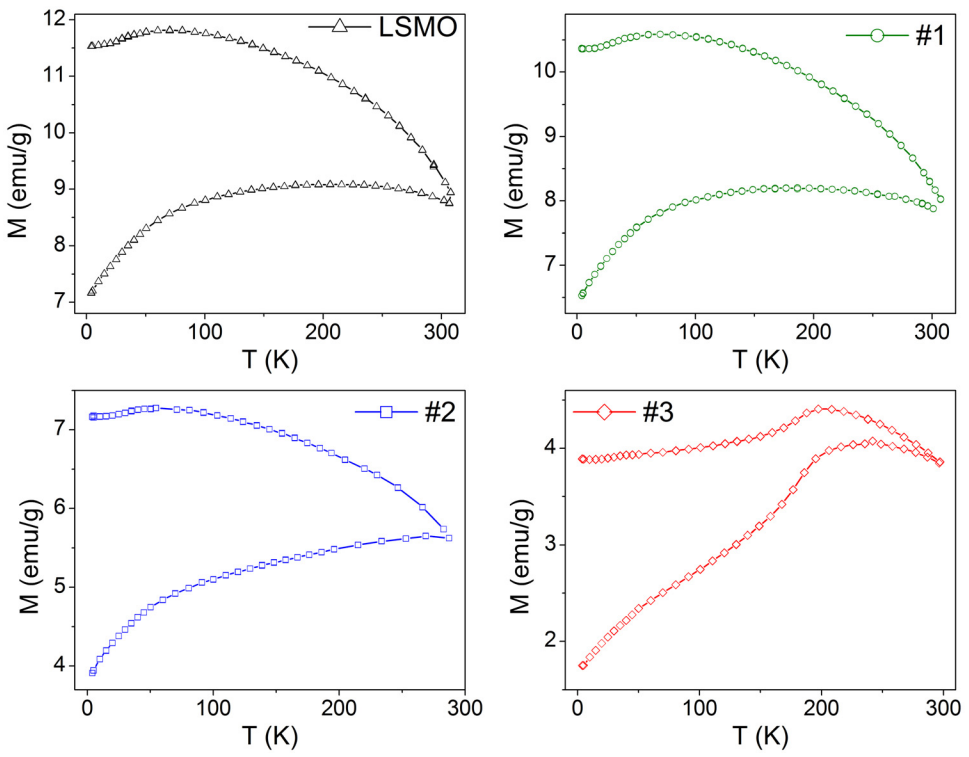

FIG. 5. (Color online) Magnetization vs temperature dependences under ZFC-FC conditions for LSMO and LSMO@PPy 1 – 3 nanocomposites. The applied magnetic field was 0.01 T.

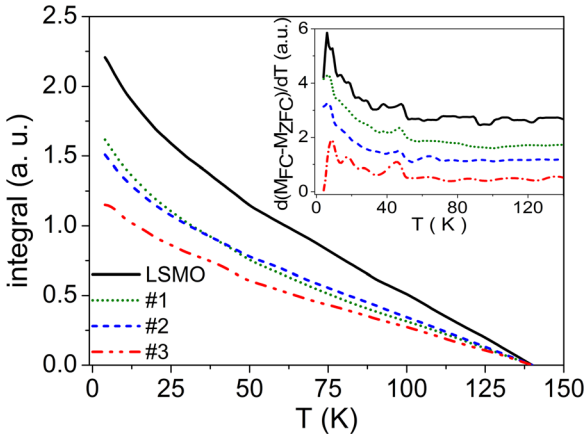

FIG. 6. (Color online) Temperature dependences of mean energy barrier heights for the LSMO sample together with the LSMO@PPy samples 1 – 3. The inset shows the energy barriers distributions of mentioned samples as resulted from first derivative of TRM.

dipole–dipole coupling of neighbor nanoparticles influence the height of the energy barrier and affects the blocking temperatures of the nanoparticles.[22–24] The temperature dependence of the total mean height of the energy barriers for a nanoparticle ensemble that are still magnetically blocked at a given temperature T, $\langle \Delta E_{tot} \rangle_T$ can be calculated by integrating the energy barrier distribution functions over the blocked states (in the upward sense starting from a given T) following Pana *et al.*[21] It reflects both anisotropy and dipolar interactions contributions in the superparamagnetic behavior, but other interactions are also contained. The calculated temperature dependences of $\langle \Delta E_{tot} \rangle_T$ for the bare LSMO sample together with PPy covered nanoparticle samples are presented in Fig. 6. Above ~40 K, the linear type dependences having negative slopes, indicating that strong dipole–dipole interactions are present between blocked nanoparticles in all the cases. The absolute value of the slope is proportional to the mean number of nearest neighbors $\langle n \rangle$.[21–24] Therefore weaker interactions (lower $\langle n \rangle$) are present in the case of LSMO@PPy sample 3, which possesses a thick polymeric shell as compared to the LSMO uncovered nanoparticles. The blocking temperatures for dependences presented in Fig. 5 are: 210 K for LSMO and 187, 268, and 241 K for samples 1 – 3, respectively. These values reflect the pure anisotropy density energy barrier coupled to the dipole–dipole magnetic interactions producing effective higher energy barriers as compared to the noninteracting situation.

A significant increase of the saturation magnetizations, M_S, for the LSMO@PPy composites as compared to the bare LSMO nanoparticles represents the second important fact as evidenced in the fourth column of Table II. Typical values of the saturation magnetization for polycrystalline Sr doped manganite ($x = 0.2 - 0.4$), at room temperature, are within 40 – 65 emu/g range,[26–28] while at lower temperatures (20 – 50 K) they rise up to around 90 emu/g.[28–30]

The increase of the saturation magnetization process arises as a direct result of PPy attachment to the nanoparticle surfaces. It should be noticed that the same type of increase of M_S has been reported for the oleic acid coating and PPy coating of magnetite nanoparticles, respectively.[5–12] It seems that the attachment of organic molecules to the surface of magnetic nanoparticles could induce a reduction of the surface spin disorder resulting in an increase of the saturation magnetization values.

In the case of the PPy coating of magnetite nanoparticles,[12] the process was correlated to a charge transfer process arising from the conducting polymer to the surface iron ions of magnetite. It involves the laterally delocalized π electrons of the conjugated PPy that could penetrate under the surface of nanoparticles.

In the present case, at the interface between polymer and the nanoparticle, the delocalized π electrons of the PPy penetrate the first atomic layers of LSMO, producing a transfer of spin paired electrons from the polymer π energy band to either Mn or O ion positions. The transfer to oxygen positions refers to surface missing or displaced O ions. The basic mechanism for ferromagnetic spin correlations in hole doped manganites ($x = 0.15 - 0.45$) is the double-exchange between Mn^{3+} and Mn^{4+} positions intermediated by p orbitals of oxygen ions. Near the surface of LSMO, due to the surface local distortions, the double-exchange correlations are broken, resulting in a disordered (uncorrelated) system of magnetic moments. In the case of magnetic nanoparticles, the uncorrelated spins form the so called outer magnetic disordered shell. This effect is important for a nanoparticle of 5 nm diameter because the first two atomic layers contain 40 – 48% of the total number of contained atoms.[31] It appears that, in the case of a LSMO nanoparticle, by adding the PPy external shell, the transferred spin paired electrons restores the double-exchange and increases the magnetic order at the surface layers, thus determining an increase of the surface contribution to the overall magnetic moment.

Additional qualitative information concerning the surface contribution to the magnetizations results by the comparative analyses of coercive field, H_C, versus temperature of nanocomposite samples together with LSMO bare nanoparticles. In Fig. 7, there are presented the temperature dependences of H_C for samples 1 – 3 together with LSMO sample. By decreasing the temperature, in case of polymer covered samples, the coercive fields begin to increase in a more pronounced manner as compared to LSMO nanoparticles. It is

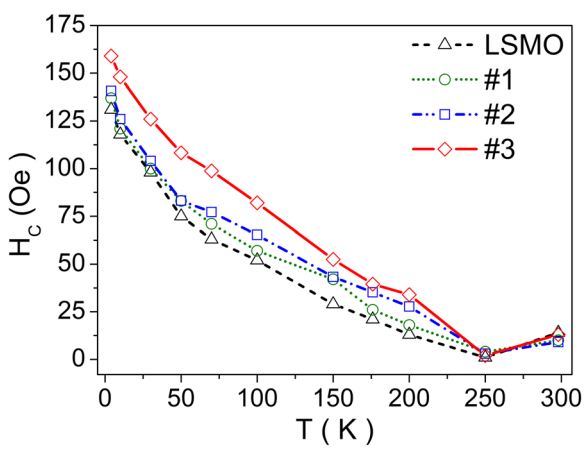

FIG. 7. (Color online) Temperature dependences of the coercive field H_C for samples 1 – 3 together with LSMO sample.

an indication that by increasing the PPy quantity, the magnetic anisotropy density also increases at all temperatures. The increase of the anisotropy density is a significant support for the increase of the magnetic ordering occurring inside the outer layers as a consequence of charge transfer from PPy. The resulting surface increased magnetic order also increases the contribution of the surface anisotropy to the total effective anisotropy density.

The third interesting observation, as it results from the last column of Table II, refers to the number of Bohr magnetons per formula unit (one Mn atom) for PPy coated LSMO nanoparticles. In case of LSMO doped at a level of $x = 0.33$, the calculated maximum number of Bohr magnetons per Mn is $\mu_S = 3.67$. From Table II, it appears that by increasing the quantity of attached polymer, the number of Bohr magnetons per Mn ion also increases until, in the case of sample 3, the value of $\mu_S = 4.24$ overcomes this maximum expected value of 3.67. Both processes can be associated with charge and spin transfer from PPy polymer to the surface layers of manganite nanoparticles. These results suggests the existence of an additional contribution to the overall magnetic moment arising from the π band itinerant electrons of PPy brought in the vicinity of surface Mn ions, which are polarized by the exchange interaction with the Hund coupled 3*d* spins of manganese ions. It is indirect evidence of the spin polarization of π energy band electrons of PPy. A similar effect was observed in the case of rare earth metals and their compounds where the atomic moments per rare earth atom are amplified as a result of 5*d* conduction electrons polarized by exchange interactions with 4*f* spins. This way, in metallic Gd, the magnetic moment per Gd atom is 7.6 Bohr magnetons, indicating an additional 0.6 Bohr magnetons contribution coming from the spin polarization of the 5*d* itinerant electrons.[32]

As it was pointed out in the preceding paragraphs, the charge transferred from PPy to LSMO can go either to manganese or empty/displaced surface O ions positions. To decide between these options, we performed XAS measurements in XANES region. The Mn-K absorption edge was investigated for the LSMO@PPy 1–3 samples. As a reference the same line was recorded for the bare LSMO nanoparticles.

Figure 8 presents results of X-ray absorption near edge structure (XANES) measurements at the Mn K-edge. To avoid superposition, the absorption spectra in Fig. 8 were upwardly displaced. The inset presents the derivative spectra, performed to prove if some chemical shifts of the absorption edge, defined as the inflection point of the XANES, appear.[33] Here the derivatives of the XANES spectra are not displaced. As one can see, no noticeable chemical shift corresponding to the transition from 1*s* to final states of *p* symmetry is observed between the LSMO and the LSMO@PPy. That means the empty DOS of *p* symmetry is not affected by the polymer adsorption. On the contrary, as can be seen in the inset of Fig. 8, by increasing the polymer quantity, the low intensity pre-edge peaks, roughly ranging from 6535 to 6550 eV, are significantly modified as referring to both positions and intensities. An example for the deconvolution of pre-edge lines is shown in Fig. 9 for LSMO@PPy 1. It was made by using a modified Voigt profile while the extraction of the baseline was realized

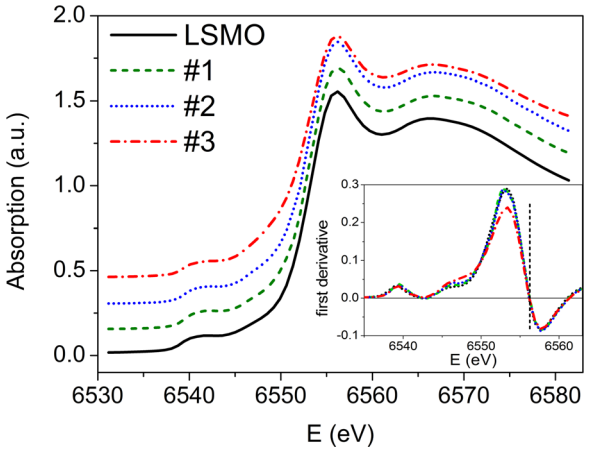

FIG. 8. (Color online) X-ray absorption near edge structure (XANES) spectra at the Mn K-edge for LSMO nanoparticles and LSMO@PPy samples 1–3. The inset presents the first derivative spectra for the same samples showing significant modifications of the pre-edge features (below 6550 eV) with increasing polymer concentrations. The vertical line indicates the position of the main transition of Mn K-edge.

by considering *spline* functions. After the extraction of the base lines, the pre-edge features for the LSMO@PPy samples and for LSMO uncoated nanoparticles are presented in Fig. 10. The line positions and integral intensities for A_1, A_2, and B components are summarized in Table III.

The lowest peaks (6537–6542 eV), labeled A_1 and A_2 as indicated by Guardia *et al.*,[5] are generally assumed to be caused by 1*s* to 3*d* transitions. Because $1s \rightarrow 3d$ transitions are dipole forbidden, they are ascribed to a mixture of $1s \rightarrow 3d$ quadrupole allowed transitions with $1s \rightarrow$ hybridized 3*d*-4*p* dipole allowed transitions.[34] At the present, doping regime LSMO is a half metal because, due the intense Hund coupling of $J_H \sim 0.7-0.8$ eV,[35] the 3*d* energy band is split into majority t_{2g} and e_g bands and minority e_g and t_{2g} empty electronic states, respectively. The splitting of the majority and minority e_g spin states results in a splitting of the Mn pre-edge features.[35]

Within this picture, the A_1 transitions involves majority partially filled e_g states while the A_2 feature is associated with the minority upper empty e_g states. The higher energy

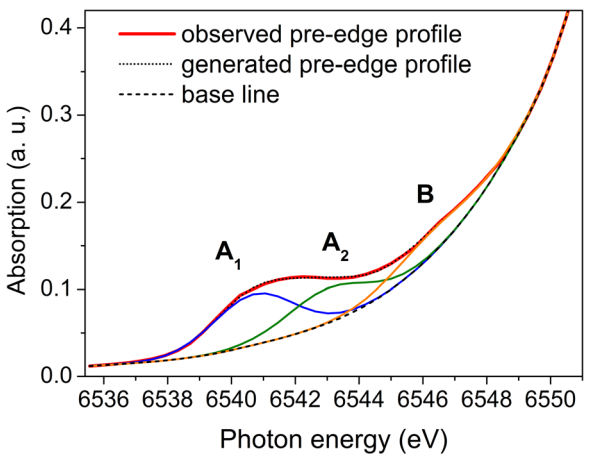

FIG. 9. (Color online) Deconvolution of pre-edge lines for LSMO@PPy sample 1. The deconvolution was made by using a modified Voigt profile while the baseline was set by considering *spline* functions.

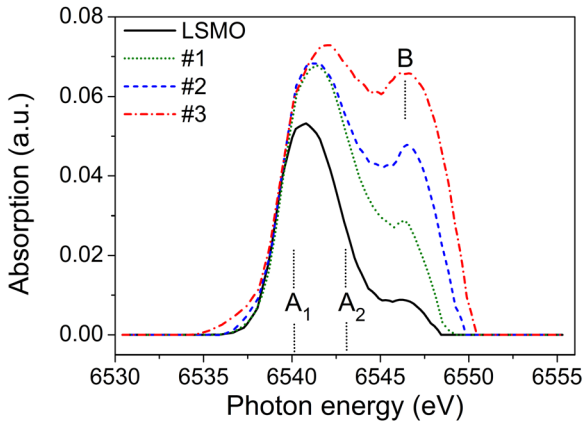

FIG. 10. (Color online) Mn-K pre-edge features for the LSMO@PPy samples and for LSMO uncoated nanoparticles after the extraction of the base lines. A_1 transitions involves majority partially filled e_g states while A_2 feature is associated to minority upper empty e_g states. The higher energy feature labeled the B is associated with Mn-4*p* states.

feature labeled the B (6543–6548 eV) is connected to the Mn 4*p* states.[34,36,37] More precisely, it is related to the Mn 4*p* local states hybridized with neighboring Mn 3*d* as calculated by Elfimov *et al.*[35] They used LSDA + U calculations with appropriate symmetry restrictions to show that a hybridization of the 4*p* states belonging to the "local" manganese ion with the 3*d* states of neighbor Mn positions is allowed. Their calculations indicate a low energy tail with features below the main edge and corresponding to the mentioned A and B peaks. They also show that the 4*p* DOS is very broad and Mn 4*p* states are highly delocalized and extend over several Mn positions.[34,38]

The oxygen *p* orbitals intermediate this hybridization resulting in spatially extended 4*p*-3*d* energy bands. At the surface of the LSMO nanoparticles, due to the distorted or missing oxygen, the partially filled $3d - e_g$ majority, 3*d* minority (empty), and 4*p*-3*d* hybridized (empty) energy bands are disrupted. When the PPy is added at the surface of nanoparticles, the charge transfer is more or less reestablished between surfaces and/or near surface Mn positions and the altered band structure is restored. Additionally, the DOS within these bands amplifies with increasing charge and spin mobility.

One can see that all A_1, A_2, and B features increase in intensity and energy position with increasing polymer content. The increase by the preceding specified intensities implies a depopulation of Mn 3*d* states, indicating that the PPy π band electrons go to oxygen positions produced by missing or displaced O ions as a consequence of the surface effects. A configuration $4s_0 3d_2$, which corresponds to Mn^{5+}, can be ruled out. Actually, the oxygen deficiency at the nanoparticle surface breaks the double-exchange between Mn ions creating some spin disordered layers hence reducing the saturation magnetization. The π electrons belonging to PPy substitute the missing oxygen and reestablish the exchange between Mn^{3+} and Mn^{4+} positions. An increase in the mobility of e_g majority electronic states accompanied by an increased bandwidth for e_g results. The above-mentioned process determines the increase of both intensity and absorption energy position of the A_1 feature. It produces an apparent increase of the Mn^{4+} content that can be correlated with the magnetization increase via the enhancement of the double-exchange interactions between manganese positions at the surface of the PPy covered nanoparticles. A noticeable enhancement of the pre-edge peak A_2 and B with increasing the polymer adsorption can be also observed. The delocalized π electrons of the PPy chains entering below the surface of the nanoparticles also reestablish the minority energy e_g band and act as a bridge for the hybridization of Mn 4*p* and neighboring Mn 3*d* states.[35] Therefore it will result an increase of the DOS within both empty minority e_g and hybridized 4*p* bands accompanied by the intensity increase of the oxygen vacancies existing at or near the surface of LSMO nanoparticles.[37] However, this effect is quite new because even changing the composition in LSMO did not show such a huge shift in the pre-edge region.[34]

IV. CONCLUSIONS

LSMO@PPy nanocomposites were obtained by the oxidative polymerization of pyrrole in presence of water dispersed LSMO nanoparticles. The polymerization produced some adhesive PPy layers around the magnetic nanoparticles, leading thus to a core-shell structure evidenced by HRTEM. The magnetization behavior, M(H) and M(T), of the composite samples is a superparamagnetic one with a very low coercitive field (~15 Oe) at room temperature. On the other hand, a significant increase of the saturation magnetizations appears for all the samples when compared to the bare LSMO nanoparticles. The surface modification of manganite nanoparticles by polypyrrole coating results in a decrease of surface spin disorder. Therefore from the synthesis point of view, the pyrrole polymerization is a relevant synthesis method that allows tailoring the magnetic properties of the LSMO nanocomposites.

Our results show for the first time that an enhancement of the magnetization could be obtained in the case of manganite nanoparticles coated with PPy due to the charge transfer from polymer π electronic states to some oxygen vacancies near the surface of the nanoparticles. This novel effect is ascribed to a

TABLE III. The line positions and integral intensities for A_1, A_2 and B components.

	A_1		A_2		A_1+A_2	B		A_1+A_2+B
Sample	Pos. (eV)	Area (a.u.)	Pos. (eV)	Area (a.u.)	Centroid (eV)	Pos. (eV)	Area (a.u.)	Centroid (eV)
LSMO	6540.41	0.157	6542.58	0.065	6541.05	6545.97	0.029	6541.61
1	6540.69	0.187	6543.01	0.128	6541.63	6546.26	0.087	6542.63
2	6540.65	0.189	6543.33	0.183	6541.97	6546.90	0.139	6543.31
3	6541.29	0.310	6545.02	0.207	6542.78	6547.69	0.150	6543.88

charge transfer process from the conducting polymer to the surface iron ions of magnetite. At high PPy concentrations, the increased number of Bohr magnetons overcomes the maximum allowed value, indicating the spin polarization of π electrons band of the conducting polymer PPy. The observed changes in the Mn-K pre-edge XANES spectrum show how, by increasing the PPy content involving an increased paired electrons transfer to the surface of LSMO nanoparticles, one has an enhanced overlapping between manganese neighbor positions that, in turn, restores the initially distorted or interrupted energy band structure for $3d\ e_g$ both majority and minority spin states. Also the hybridization of "local" $4p$ orbital with neighbor Mn $3d$ orbital and associated band formation are favored. These specific behaviors of the nanocomposite samples, as compared to bare nanoparticles, support the existence of a spin paired charge transfer from PPy to the manganite nanoparticles.

The easy polymerization of PPy in stable dispersions of magnetic nanoparticles represents a good strategy to generate magnetic nanocomposites with controllable magnetic properties, which can be further easily provided with biofunctionality by the attachment of specific molecular groups to the polymer chains for applications in biotechnology.

ACKNOWLEDGMENTS

This work was funded by the National Council for Scientific Research under the Contracts CNCS PCCE ID_76/2010 and ID_119/2011. We acknowledge valuable help from the Hasylab beamline scientist Dr. Edmund Welter.

[1]R. Gangopadhyay and A. De, Chem. Mater. **12**, 608 (2000).
[2]R. Turcu, O. Pana, A. Nan, and L. M. Giurgiu, *Polymeric Nanostructures and Their Applications*, edited by H. S. Nalwa (American Scientific Publishers, Stevenson Ranch, CA, 2007), Vol. 1, pp. 337–399.
[3]X. Batle and A. Labarta, J. Phys. D **35**, R15 (2002).
[4]M. Blanco-Mantecón and K. O'Grady, J. Magn. Magn. Mater. **296**, 124 (2006).
[5]P. Guardia, B. Batlle-Brugal, A. G. Roca, O. Iglesias, M. P. Morales, C. J. Serna, A. J. Labarta, and X. Batlle, J. Magn. Magn. Mater. **316**, e756 (2007).
[6]L. Del Bianco, D. Fiorani, A. M. Testa, E. Bonetti, L. Savini, and S. Signoretti, Phys. Rev. B **66**, 174418 (2008).
[7]J. L. Dormann, F. D'Orazio, F. Lucari, E. Tronc, P. Prene, J. P. Jolivet, D. Fiorani, R. Cherkaoui, and M. Nogues, Phys. Rev. B **53**, 14291 (1996).
[8]B. Martinez, X. Obradors, L. Balcells, A. Rouanet, and C. Monty, Phys. Rev. Lett. **80**, 181 (1998).
[9]J. M. Vargas, L. M. Socolovsky, M. Knobel, and D. Zanchet, Nanotechnology **16** S285 (2005).
[10]T. N. Shendruk, R. D. Desautels, B. W. Southern, and J. van Lierop, Nanotechnology **18**, 455704 (2007).
[11]J. Pyun, Polym. Rev. **47**, 231 (2007).
[12]R. Turcu, O. Pana, A. Nan, I. Craciunescu, O. Chauvet, and C. Payen, J. Phys. D **41**, 24502 (2008).
[13]Y. H. Huang, C. H. Yan, Z. M. Wang, C. S. Liao, and G. X. Xu, Solid State Commun. **118**, 541 (2001).
[14]Y. H. Huang, Z. G. Xu, C. H. Yan, Z. M. Wang, T. Zhu, C. S. Liao, S. Gao, and G. X. Xu, Solid State Commun. **114**, 43 (2000).
[15]J. Mahía, C. Vázquez-Vázquez, J. Mira, M. A. López-Quintela, J. Rivas, T. E. Jones, and S. B. Oseroff, J. Appl. Phys. **75**, 6757 (1994).
[16]R. D. Sánchez, J. Rivas, C. Vázquez-Vázquez, M. A. López-Quintela, M. T. Causa, M. Tovar, and S. Oseroff, Appl. Phys. Lett. **68**, 134 (1996).
[17]A. J. Nelson, J. G. Reynolds, and J. W. Roos, J. Vac. Sci. Technol. **A18**, 1072 (2000).
[18]P. J. Cumpson and M. P. Seah, Surf. Interface. Anal. **25**, 430, (1997).
[19]I. S. Jacobs and C. P. Bean, *Magnetism*, edited by G. T. Rado and H. Suhl (Academic, New York, 1963), Vol. 3, pp. 271–349.
[20]R. W. Chantrell, J. Popplewell, and S. W. Charles, IEEE Trans. Magn. **14**, 975 (1978).
[21]O. Pana, R. Turcu, M. L. Soran, C. Leostean, E. Gautron, C. Payen, and O. Chauvet, Synth. Met. **160**, 1692 (2010).
[22]M. El-Hilo, K. O'Grady, and R. W. Chantrell, J. Magn. Magn. Mater. **114**, 295 (1992).
[23]S. Shtrikman and E. P. Wohlfarth, Phys. Lett. A **85**, 467 (1981).
[24]J. L. Dormann, L. Bessasis, and D. Fiorani, J. Phys. C **21**, 2015 (1988).
[25]L. Néel, C.R. Acad. Sci., Paris **228**, 664 (1949).
[26]J. Mira, J. Rivas F. Rivadulla, C. Vázquez-Vázquez, and M. A. López-Quintela, Phys. Rev. B **60**, 2998 (1999).
[27]M. P. Gutiérrez, J. H. Olivares, I. Betancourt, and F. Morales, J. Mater. Res. **24**, 1585 (2009).
[28]I. P. Muthuselvam and R. N. Bhowmik, J. Alloy. Compd. **511**, 22 (2012).
[29]G. H. Jonker, Physica XXII, 707 (1956).
[30]S. Zemni, A. Gasmia, M. Boudard, and M. Oumezzine, Mater. Sci. Eng. B Solid **144**, 117 (2007).
[31]J. L. Dormann, D. Fioriani, and E. Tronc, *Advances in Chemical Physics*, edited by I. Prigogine and Stuart A. Rice (Wiley and Sons, New York, 1997), Vol. XCVIII, pp. 283–494.
[32]B. Kim, A. B. Andrews, J. L. Erskine, K. J. Kim, and B. N. Harmon, Phys. Rev. Lett. **68**, 1931 (1992).
[33]B. K. Teo, *EXAFS: Basic Principles and Data Analysis* (Springer -Verlag, Berlin, 1986).
[34]F. Bridges, C. H. Booth, G. H. Kwei, J. J. Neumeier, and G. A. Sawatzky, Phys. Rev. B **61**, R9237 (2000).
[35]I. S. Elfimov, V. I. Anisimov, and G. A. Sawatzky, Phys. Rev. Lett. **82**, 4264 (1999).
[36]M. Croft, D. Sills, M. Greenblatt, C. Lee, S.-W. Cheong, K. V. Ramanujachary, and D. Tran, Phys. Rev. B **55**, 8726 (1997).
[37]P. Ghigna, A. Carollo, G. Flor, L. Malavasi, and G. Subias Peruga, J. Phys. Chem. B **109**, 4365 (2005).
[38]G. Subías, J. Garcíía, M. G. Proietti, and J. Blasco, Phys. Rev. B **56**, 8183 (1997).